44th AIAA Aerospace Sciences Meeting and Exhibit
9 - 12 January 2006, Reno, Nevada

AIAA 2006-152

Large Eddy Simulation of Bluff Body Stabilized Premixed Flame

Ionut Porumbel* and Suresh Menon†

School of Aerospace Engineering, Georgia Institute of Technology, Atlanta, Georgia, 30332, USA

This paper presents results of numerical simulations of cold and reactive flow behind a bluff body, in comparison with experimental data. The results of the non-reacting flow are found in good agreement with the experiments. For the reactive flow, two closures for the filtered scalar transport equations are used: a conventional closure at the LES resolved scale, based on the sub-grid Eddy Break-Up (EBU) model, and a closure directly at the sub-grid scales, the Linear Eddy Mixing (LEM) model. Although the time-averaged velocity fields are in close agreement with the experimental data for both simulations, the EBU flame is thicker and fails to adapt to the turbulent fluctuations in the flow field. Therefore, EBU model under-predicts the turbulent flame wrinkling and the far-field wake spread. Also, EBU underpredicts the centerline temperature values, due to an under-prediction in the turbulent mixing rate.

I. Introduction

Due to the wide range of aeronautical applications, bluff body stabilized flames have been an important research topic for quite a long time. Experimental studies investigating the flow pattern in the wake of bluff bodies in reactive and non-reactive flows have been conducted for more than 50 years, and a detailed review of the early work on bluff body stabilized flames can be found in the review article by Ozawa.[1] Detailed flow measurements were conducted by Sjunesson et al.[2–4] at VOLVO (Sweden) as part of a research program intent to further the understanding of turbulent premixed flames and to develop a database for validation of combustion models.

From a numerical standpoint, the use of Direct Numerical Simulations (DNS) for high, or even moderate, Reynolds number flows remains unattainable due to computational limitation. Reynolds Averaged Navier Stokes (RANS) methods for reactive flows behind bluff bodies have been conducted by many researchers (e.g. Bai and Fuchs[5]), but important discrepancies were observed due to shortcomings inherent in the RANS methodology, especially in complex flows. A promising tool for the study of reactive flows in complex geometries is Large Eddy Simulation (LES). In LES, the three dimensional large scale motion is resolved, hence the non-universal, geometry dependent flow features are captured accurately, and only the small scales that exhibit local isotropy are modelled. In the cases studied here, the two boundary layers that form on the two sides of the bluff body separate at the bluff body edge and form a pair of free shear layers surrounding a central recirculation region. The flow dynamics are largely controlled by the large scale fluctuations, caused by large eddies, often called *coherent structures*.[6] Therefore, the mean fields alone, as resolved by RANS methods, are insufficient for accurate predictions. Also, previous studies[7] have also shown that the full compressible LES equations (as employed in this study) allow the accurate capture of acoustic-vortex-entropy interactions that are expected to play a critical role in the flame stabilization mechanism behind a bluff body. Significantly improved LES results have been obtained in the past to support this claim.[8–10]

The goal of the present study is to accurately simulate a stable, premixed, reacting flow behind a bluff body using a LES approach. The first section gives a brief presentation of the governing equations, the LES filtering, and the closure models. Next, the numerical procedure is described, followed by results of a non reactive flow simulation, that are compared to the experimental observations in order to validate the numerical algorithm. Finally, two reactive flow simulations, one employing the Linear Eddy Mixing

*Graduate Research Assistant, AIAA Student Member, ionut_porumbel@ae.gatech.edu
†Professor, AIAA Associate Fellow, suresh.menon@ae.gatech.edu

(LEM) closure and another one employing a closure at the LES resolved scale based on the Eddy Break-Up (EBU) model are discussed and compared with each other, and against the experimental data existing in the literature. The accuracy and limitations of each model are assessed and discussed in light of their respective ability to capture key features of the turbulent reactive flow.

II. Problem Formulation

The Favre filtered LES equations are:[11]

$$\begin{cases} \frac{\partial \overline{\rho}}{\partial t} + \frac{\partial \overline{\rho}\widetilde{u_i}}{\partial x_i} = 0 \\ \frac{\partial \overline{\rho}\widetilde{u_i}}{\partial t} + \frac{\partial}{\partial x_j}\left[\overline{\rho}\widetilde{u_i}\widetilde{u_j} + \overline{p}\delta_{ij} - \overline{\tau_{ij}} + \tau_{ij}^{sgs}\right] = 0 \\ \frac{\partial \overline{\rho}\widetilde{E}}{\partial t} + \frac{\partial}{\partial x_i}\left[\left(\overline{\rho}\widetilde{E} + \overline{p}\right)\widetilde{u_i} + \overline{q_i} - \widetilde{u_j}\overline{\tau_{ij}} + H_i^{sgs} + \sigma_i^{sgs}\right] = 0 \\ \frac{\partial \overline{\rho}\widetilde{Y_m}}{\partial t} + \frac{\partial}{\partial x_i}\left[\overline{\rho}\widetilde{Y_m}\widetilde{u_i} + \overline{\rho}\overline{D}_m\frac{\partial \widetilde{Y_m}}{\partial x_i} + \Phi_{i,m}^{sgs} + \theta_{i,m}^{sgs}\right] = \overline{\dot{w}}_m, m = 1, N \\ \overline{p} = \overline{\rho}R\widetilde{T} + T^{sgs} \end{cases} \quad (1)$$

In the above, the symbol $\widetilde{f}$ represents the Favre (density weighted) spatial filtering of any quantity f and the overbar stands for the spatial filtering. The filter width is the grid size, $\overline{\Delta}$. Here, t is the time, x_i is the spatial coordinate, δ_{ij} is the Kronecker symbol, ρ is the mass density, p is the pressure, T is the temperature, $R = \sum_{m=1}^{N} Y_m R_u/W_m$ is the gas constant, R_u is the universal gas constant, Y_m is the mass fraction of chemical species m, W_m its molecular mass, N is the total number of chemical species, u_i is the velocity vector, and $E = e + u_{kk}^2/2$ is the total energy per unit mass, where $e = \sum_{m=1}^{N} Y_m h_m - p/\rho$ is the internal energy, and h_m is the species enthalpy, given by the caloric equation of state:

$$h_m = \Delta h_{f,m}^0 + c_{p,m}(T - T^0) \quad (2)$$

where $\Delta h_{f,m}^0$ is the species standard heat of formation at temperature T^0 and $c_{p,m}$ the species specific heat at constant pressure. Also, τ_{ij} is the viscous stress tensor, and D_m is the molecular diffusion coefficient of the m-th species, The filtered heat flux vector, q_i is:

$$\overline{q_i} = -\overline{\kappa}\frac{\partial \widetilde{T}}{\partial x_i} - \overline{\rho}\sum_{m=1}^{N}\widetilde{h_m}\overline{D}_m\frac{\partial \widetilde{Y_m}}{\partial x_i} + \sum_{m=1}^{N} q_{i,m}^{sgs} \quad (3)$$

The filtered LES equations contain unknown terms representing the effects of the unresolved scales on the resolved motion and denoted by the superscript sgs:

- the sub-grid stress tensor $\tau_{ij}^{sgs} = \overline{\rho}[\widetilde{u_i u_j} - \widetilde{u_i}\widetilde{u_j}]$;
- the sub-grid enthalpy flux $H_i^{sgs} = \overline{\rho}[\widetilde{Eu_i} - \widetilde{E}\widetilde{u_i}] + \overline{pu_i} - \overline{p}\widetilde{u_i}$;
- the sub-grid viscous work $\sigma_i^{sgs} = \overline{u_j\tau_{ij}} - \widetilde{u_j}\overline{\tau_{ij}}$;
- the sub-grid convective mass flux $\Phi_{i,m}^{sgs} = \overline{\rho}[\widetilde{u_i Y_m} - \widetilde{u_i}\widetilde{Y_m}]$;
- the sub-grid diffusive mass flux $\theta_{i,m}^{sgs} = \overline{\rho}[\widetilde{V_{i,m}Y_m} - \widetilde{V_{i,m}}\widetilde{Y_m}]$;
- the sub-grid heat flux $q_{i,m}^{sgs} = \overline{h_m D_m \partial Y_m/\partial x_i} - \widetilde{h}_m\overline{D}_m\partial\widetilde{Y}_m/\partial x_i$;
- the sub-grid temperature-species correlation $T^{sgs} = \sum_{m=1}^{N}\left(\widetilde{Y_m T} - \widetilde{Y_m}\widetilde{T}\right)/W_m$;

Also unknown at this point is the filtered reaction rate, $\overline{\dot{w}}_m$.

To achieve closure for the these terms a non-equilibrium eddy viscosity model is used. The model is based on solving a localized dynamic model for the sub-grid kinetic energy, k^{sgs}, along with the LES equations. The sub-grid kinetic energy transport equation is given by:

$$\frac{\partial \overline{\rho}k^{sgs}}{\partial t} + \frac{\partial}{\partial x_i}(\overline{\rho}\widetilde{u_i}k^{sgs}) = P^{sgs} - \epsilon^{sgs} + \frac{\partial}{\partial x_i}\left(\overline{\rho}\frac{\nu_T}{\sigma_k}\frac{\partial k^{sgs}}{\partial x_i}\right) \quad (4)$$

In the above, σ_k is set to 0.9 for this study. The terms P^{sgs} and ϵ^{sgs} are, respectively, the production and the dissipation of sub-grid kinetic energy and are modelled as:

$$P^{sgs} = -\tau_{ij}^{sgs}\frac{\partial \widetilde{u_i}}{\partial x_j} \tag{5}$$

and:

$$\epsilon^{sgs} = C_\epsilon \frac{(k^{sgs})^{3/2}}{\overline{\Delta}} \tag{6}$$

This model does not assume equilibrium at the sub-grid scales, and the characteristic velocity scale in the eddy viscosity model is explicitly computed. Thus, the turbulent viscosity, ν_T, is modelled as:

$$\nu_T = C_\nu \sqrt{k^{sgs}}\overline{\Delta} \tag{7}$$

Here, C_ν and C_ϵ are the model coefficients, computed using a localized dynamic model,[12] that adapts them to the local flow characteristics based on the scale similarity hypothesis in the inertial range. With the sub-grid kinetic energy known, the sub-grid stress tensor is given by:

$$\tau_{ij}^{sgs} = -2\overline{\rho}\nu_T\Big(\widetilde{S}_{ij} - \frac{1}{3}\widetilde{S}_{kk}\delta_{ij}\Big) + \frac{2}{3}\overline{\rho}k^{sgs}\delta_{ij} \tag{8}$$

where $\widetilde{S}_{ij} = (1/2)(\partial\widetilde{u}_i/\partial x_j + \partial\widetilde{u}_j/\partial x_i)$ is the resolved rate of strain.

The sub-grid enthalpy flux is modelled using the eddy viscosity model as:

$$H_i^{sgs} = -\frac{\overline{\rho}\nu_T}{Pr_t}\frac{\partial \widetilde{H}}{\partial x_k} \tag{9}$$

where $\widetilde{H}$ is the total enthalpy per unit mass, $\widetilde{H} = \widetilde{E} + \overline{p}/\overline{\rho}$ and Pr_t is the turbulent Prandtl number, set to unity here.

The sub-grid viscous work, σ_i^{sgs}, is neglected.[13] Thus, the closure for LES conservation of mass, momentum and energy is achieved with no parameters to explicitly tune or adjust.

III. Combustion Modelling

Several terms in Eqs. (1) and (3) still remain open at this point: the sub-grid convective ($\Phi_{i,m}^{sgs}$) and diffusive ($\theta_{i,m}^{sgs}$) species fluxes, the sub-grid heat flux, $q_{i,m}^{sgs}$, the sub-grid temperature-species correlation, T^{sgs} and the filtered reaction rate, $\overline{\dot{w}}_m$. In this study, two approaches towards closing these terms are considered: a conventional closure at the LES resolved scale and a closure directly at the sub-grid scales.

The conventional closure for the species equations employs for the sub-grid convective scalar flux an eddy diffusivity closure, $D_T = \nu_T/Sc_T$, where Sc_T is a turbulent Schmidt number that was set to unity in this study. Note that, since ν_T is obtained dynamically, D_T is also dynamically obtained in this closure. Thus:

$$\Phi_{i,m}^{sgs} = -\frac{\overline{\rho}\nu_T}{Sc_T}\frac{\partial \widetilde{Y_k}}{\partial x_i} \tag{10}$$

Since no conventional closure models exist[14] for the sub-grid heat flux, $q_{i,m}^{sgs}$, the sub-grid diffusive species flux, $\theta_{i,m}^{sgs}$ and the sub-grid temperature-species correlation, T^{sgs}, these terms have been neglected at present.

Although many models for the filtered reaction rate have been proposed, especially for premixed combustion,[15,16] this study uses an approach based on a sub-grid EBU approach developed earlier by Fureby and Moller.[13] The basic idea is that for combustion to occur, two processes need to take place simultaneously: chemical reaction and scalar mixing, and the rate controlling phenomena will be the slower of the two. The turbulent mixing rate is given by:[17]

$$\overline{\dot{\omega}_p} = \overline{\rho}C_{EBU}\frac{\varepsilon}{k}\overline{Y_F} \tag{11}$$

where ε is the turbulent dissipation, k is the turbulent kinetic energy, $\overline{Y_F}$ is the minimum reactant mean mass fraction and C_{EBU} is a model constant, set to 2 in this study.[18]

The approach is cost effective and easy to implement since the sub-grid turbulent mixing time scale can be directly estimated using k^{sgs}. Since the effects of the super-grid turbulence on the scalar fields are

resolved, k in Eq. (11) can be replaced by the known sub-grid kinetic energy, k^{sgs}, and ε by ε^{sgs}, given by Eq. (6). Hence, the mixing rate equation (which is dynamic, since k^{sgs} is dynamically obtianed) becomes:

$$\overline{\dot{\omega}_p} = \overline{\rho} C_{EBU} C_\epsilon \frac{\sqrt{k^{sgs}}}{\overline{\Delta}} \overline{Y_F} \tag{12}$$

The chemical reaction rate is given by a 5-species, 1-step, reduced chemical mechanism:

$$C_3H_8 + 5O_2 \Longleftrightarrow 3CO_2 + 4H_2O \tag{13}$$

with a reaction rate given by:[19]

$$\overline{\dot{\omega}_c} = \frac{\chi_m W_m}{\overline{\rho}} Kexp\Big(- \frac{E_a}{R_{u,cgs}\widetilde{T}}\Big)[C_3H_8]^{c_1}[O_2]^{c_2} \tag{14}$$

where χ_m is the stoichiometric coefficient, K is a pre-exponential factor equal to 8.6 x 10^{11}, E_a is the activation energy, equal to 3.0 x 10^4 cal/g, $R_{u,cgs}$ is the universal gas constant expressed in $calories/gram \cdot Kelvin$, $[X]$ represents the molar concentration of species X, in $moles/cm^3$, and c_1 and c_2 are two coefficients, set to 0.1, respectively 1.65 for this case.[19]

Finally, the smallest of these two rates is used to represent the filtered reaction rate, $\overline{\dot{\omega}_m}$. Although this approach (called EBULES hereafter) can, in many cases, provide reasonable results,[13] it also has well known limitations. First, it must be noted that small-scale scalar mixing, molecular diffusion and chemical kinetics all occur at the small scales and are not resolved in LES. Furthermore, the scalar fields at the sub-grid level are, unlike the turbulent scales, strongly anisotropic, thus rendering the use of the eddy diffusivity closure questionable. Also, in the turbulent regions, the reaction rate is independent of the actual kinetics and an over-estimation of the rate is likely to occur in regions of very high shear. In regions of low turbulence, or for very high grid resolutions approaching DNS, the sub-grid energy decreases towards zero. If the molecular diffusion effect is neglected, on grounds that it is much smaller than the turbulent mixing, the mixing rate given by Eq. (11) will tend to zero, and so will the filtered reaction rate. In spite of all these limitations, EBULES is a good baseline approach to obtain quick estimates of the combustion process, as shown in the next section.

A more comprehensive closure of the scalar mixing and combustion is based on the LEM model proposed by Kerstein,[20] and developed into a sub-grid model by Menon et al.[21] This approach, called LEMLES hereafter, has been developed in the past few years to offer a closure directly at the sub-grid scales for all combustion processes. It has been successfully applied to scalar mixing,[22–24] premixed combustion,[25–27] non-premixed combustion,[22,28] pollutant emission[27] and spray combustion,[29,30] with little or no change to the basic structure of the model.

LEM is a stochastic approach aimed at simulating, rather than modelling the effects of turbulence on the chemistry, and it is not limited by the scale separation hypothesis.[17] The parameters controlling the LEM turbulent mixing model require only the validity of the Reynolds number independence of free shear flows in the limit of large Reynolds numbers, which is a safe assumption for any flow of engineering interest.[17] Due to this extended validity range, the LEM model can be expected to perform well in any combustion regime, and to be able to accurately handle flames near to, or even outside, the flammability limits.

In LEMLES, the scalar equations are not filtered, and instead the large scale advection, turbulent mixing by eddies smaller than the grid size, molecular diffusion and chemical reaction are resolved at their appropriate length and time scales inside each LES cell. While the LES filtered conservation equations for mass, momentum and energy are numerically integrated on the LES grid, the evolution of the species fields is tracked using a two-scale, two-time numerical approach.

For any scalar an exact and unfiltered Eulerian transport equation can be written as:

$$\rho\frac{\partial\psi}{\partial t} = -\rho u_i \frac{\partial\psi}{\partial x_i} - \frac{\partial}{\partial x_i}\Big(- \rho D_\psi \frac{\partial\psi}{\partial x_i}\Big) + \dot{\omega}_\psi \tag{15}$$

where the first right hand side term represents the total convection, the second is the molecular diffusion (D_ψ is the species dependent diffusion coefficient) and the last term is the unfiltered chemical reaction source term. The velocity vector can be decomposed into:

$$u_i = \underbrace{\widetilde{u}_i}_{I} + \underbrace{\Big(u_i'\Big)^{face}}_{II} + \underbrace{u_i''}_{III} \tag{16}$$

where term (I) represents the LES resolved velocity, term (II) is the sub-grid velocity normal to the control volume surface, obtained from k^{sgs}, and term (III) is the small scale velocity fluctuation, unresolved at the LES level. By using Eq. (16) and regrouping the terms in Eq. (15), equations characterizing the large (Eq. (17)), respectively small scale processes (Eq. (18)) can be written:

$$\rho\frac{\psi^* - \psi^n}{\Delta t_{LES}} + \rho\widetilde{u}_i\frac{\partial\psi^n}{\partial x_i} + \rho\Big(u_i'\Big)^{face}\frac{\partial\psi^n}{\partial x_i} = 0 \tag{17}$$

$$\psi^{n+1} = \psi^* + \int_t^{t+\Delta_{LES}} -\frac{1}{\rho}\left[\rho u_i''\frac{\partial\psi^n}{\partial x_i} - \frac{\partial}{\partial x_i}\left(\rho D_\psi\frac{\partial\psi^n}{\partial x_i}\right) - \dot{\omega}_\psi\right]dt \tag{18}$$

In the above, Δt_{LES} is the LES time step, ψ^n and ψ^{n+1} are consecutive time values of the scalar ψ evolution, ψ^* is an intermediate solution, after the large scale convection is completed. In Eq. (18), the first term under the integral represents the sub-grid stirring, the second is the sub-grid molecular diffusion and the last accounts for the reaction kinetics.

The molecular diffusion and the chemical reaction contribution to the small scale transport are resolved on a one-dimensional grid inside each LES cell at a resolution much finer than the LES resolution, and approaching the Kolmogorov scale. The 1-D computational domain is aligned in the direction of the flame normal inside each LES cell, ensuring an accurate representation of flame normal scalar gradients.[20] On this domain (denoted the LEM domain hereafter) molecular diffusion (term A below), chemical reactions (term B), diffusion of heat via species molecular diffusion (term C), heat diffusion (term D) and chemical reaction heat release (term E) are resolved, according to the equations below:

$$\rho^{LEM}\frac{\partial Y_m^{LEM}}{\partial t} + F_m^{stir} + \underbrace{\frac{\partial}{\partial s}\Big(-\rho^{LEM}D_m\frac{\partial Y_m^{LEM}}{\partial s}\Big)}_{A} = \underbrace{\dot{w}_m W_m}_{B} \tag{19}$$

$$\rho^{LEM}c_P\frac{\partial T^{LEM}}{\partial t} + F_T^{stir} - \underbrace{\sum_{k=1}^{N}\rho c_{p,m}D_m\Big(\frac{\partial Y_m^{LEM}}{\partial s}\Big)\Big(\frac{\partial T^{LEM}}{\partial s}\Big)}_{C} - \underbrace{\frac{\partial}{\partial s}\Big(\overline{\kappa}\frac{\partial T^{LEM}}{\partial s}\Big)}_{D} = \underbrace{-\sum_{m=1}^{N}h_m\dot{w}_m W_m}_{E} \tag{20}$$

Here, the superscript LEM indicates values at the sub-grid, LEM, level, s is the spatial coordinate along the LEM domain, F_m^{stir} and F_T^{stir} represent the effect of the sub-grid turbulence on the species m mass fraction field, respectively on the temperature field.

The gas is assumed calorically perfect and the sub-grid pressure, p^{LEM} is assumed constant over the LEM domain, and equal to the supergrid value, $\overline{p}$, which is a valid assumption in the absence of strong pressure gradients.[31] Hence, the sub-grid density is computed from the equation of state at the sub-grid level :

$$p^{LEM} = \rho^{LEM}T^{LEM}\sum_{k=1}^{N}Y_k^{LEM}\frac{R_u}{W_k} \tag{21}$$

Radiation effects are neglected. The small-scale turbulent stirring (F_m^{stir} and F_T^{stir}) is implemented explicitly on the same grid using stochastic re-arrangement events that mimic the action of an eddy upon the scalar field using a method known as *triplet mapping* and designed to recover the 3D inertial range scaling laws.[20,32] The location of this stirring event is chosen from a uniform distribution. The frequency at which stirring events occur is given by:[20]

$$\lambda = \frac{54}{5}\frac{\nu Re_{\overline{\Delta}}}{C_\lambda\overline{\Delta}^3}\frac{[(\overline{\Delta}/\eta)^{5/3} - 1]}{[1 - (\eta/\overline{\Delta})^{4/3}]} \tag{22}$$

where C_λ stands for the scalar turbulent diffusivity, set to 0.067.[23]

The eddy size, l, ranges from the Kolmogorov scale, η, to the grid size, $\overline{\Delta}$ with a distribution given by:[20]

$$f(l) = \frac{(5/3)l^{-8/3}}{\eta^{-5/3} - \overline{\Delta}^{-5/3}} \tag{23}$$

where the Kolmogorov scale is determined as $\eta = N_\eta \overline{\Delta} Re_{\overline{\Delta}}^{-4/3}$ and N_η is an empirical constant that reduces the effective range of scales between the integral length scale and η but without altering the turbulent diffusivity.[32] The value used for this study is 5.[32]

Equation (17) is modelled using a Lagrangian transport of the scalar field across the LES cells that ensures exact mass conservation.[31] Thus, once the LES computations are completed at a given time step, LEM domain cells (and/or cell fractions) are exchanged between the LES cells in a manner that accounts for the mass fluxes across the LES cell faces. The volume of each LEM cell is modified after each LEM step in order to account for the volumetric expansion due to the temperature change induced by the chemical heat release. After this is completed, the LEM domain is re-gridded to maintain a constant cell volume over the entire LEM domain. Finally, the sub-grid scalar fields in each LES cell are ensemble averaged to obtain the LES-resolved scalar field, $\widetilde{Y_k}$, which is used in the LES energy equation and equation of state. Further details on the LEMLES numerical implementation and the underlying assumptions can be found in the above cited references.

It is important to note that the LEMLES employed here has no ad hoc adjustable parameters for either momentum or scalar transport equations. The k^{sgs} model plays a critical role in the LEM closure by providing estimates for the sub-grid turbulence level needed for both small-scale stirring and large-scale transport.[25] Also, since reaction kinetics and scalar mixing are used directly, without filtering, LEMLES can account for the scalar anisotropy in the small-scale.[11] Additionally, for premixed systems, it is possible to actually predict the turbulent burning rate in the sub-grid rather than just a priori specifying it, as is done in many flame speed models.[33,34] When the local turbulence level is high, the premixed flame structure can change from corrugated flamelet to thin-reaction-zone to broken-reaction-zone regime without requiring any model changes.[35] This ability is particularly important when attempting to simulate flame stability near the lean-blow-out limit.[27]

Nevertheless, the approach has some limitations. Most importantly, LEMLES is relatively much more expensive than conventional LES models, such as EBULES. However, it is highly scalable, so the overall computation time can be decreased by increasing the number of processors. Laminar molecular diffusion *across* LES cells is not included but this limitation is significant only in laminar regions, whereas LEMLES is designed for high Reynolds number turbulent flow applications. Also, the viscous work is neglected in the sub-grid temperature equation, Eq. (20), but it is explicitly included in the LES energy equation, Eq. (1c) which is used to ensure total energy conservation. Finally, the flame curvature effect is not explicitly present in the sub-grid. If the flame is highly wrinkled in the sub-grid, multiple flames can be present in the 1D line, and the distance between the flames can be approximated as twice the local radius of curvature.[36] However, this situation will only occur if the LES grid is very coarse in regions of very high turbulence, where the LES of momentum transport is expected to fail much before any sub-grid flame related effects become prominent. For the cases simulated here, the LES resolution is chosen to reasonably resolve the turbulence in the flame holding region (see next section). As a result, most (if not all) of the flame curvature effects are resolved at the LES level.

IV. Numerical Implementation

The LES filtered Navier-Stokes Eqs. (1), together with the sub-grid kinetic energy transport Eq. (4) are solved using a finite volume, cell centered, second order accurate scheme on a multiblock, body fitting grid, using a numerical algorithm based on a 5 stage modified Runge-Kutta scheme, following the work of Jameson et al.[37] The algorithm convergence is accelerated using a dual time stepping technique.[38] To eliminate spurious fluctuations of the state vector, second and fourth order artificial dissipation terms, based on pressure, are added to the residual term.[37]

The boundary conditions used here are a combination of Dirichlet and Neumann boundary conditions and can be classified in two categories: viscous, isothermal, wall boundary conditions, and inflow-outflow boundary conditions, treated according to the method developed by Baum et al.[39] for reactive, compressible, three-dimensional flows. For the inflow, the gas density is computed based on the flow information, while all other values are specified. At the outflow, second-order-accurate, partially reflecting conditions are enforced

by allowing a pressure wave coming from downstream to enter the computational domain. The amplitude of the wave is related to the difference in pressure between the outflow and the infinity downstream pressure (that must be specified). Details on the procedure will not be given here but can be found in the cited work.

The geometry of the simulations herein reproduces the *Volvo experiment*.[3] It consists of a rectangular duct of size 1.0 m x 0.24 m x 0.12 m with a triangular prism that extends between the two lateral walls of the combustor, as shown in figure 2. The side of the bluff body triangular base, a, measures 0.04 m. The computational domain was divided into 10 blocks, and each block was divided by a body fitting grid with dimensions given in Table 1 and positioned according to figure 1. For the reactive flow the spanwise resolution was increased to resolve the three-dimensional flame structure.

Block	**I**	**J**	**K (CF/RF)**	**Block**	**I**	**J**	**K (CF/RF)**
1	45	52	25/90	**6**	90	81	25/90
2	35	52	25/90	**7**	45	52	25/90
3	278	52	25/90	**8**	35	52	25/90
4	90	52	25/90	**9**	278	52	25/90
5	278	81	25/90	**10**	90	52	25/90

Table 1. Computational grid dimensions. CF = Cold Flow; RF = Reactive Flow

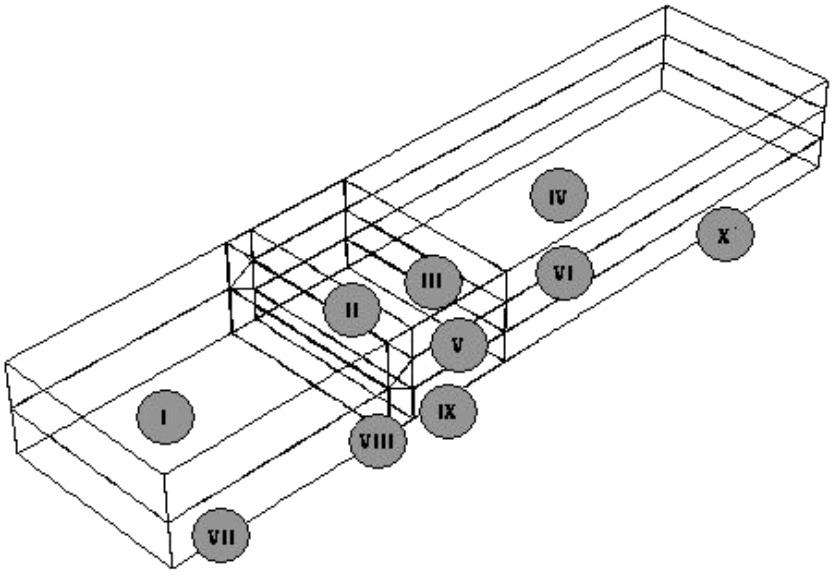

Figure 1. Spatial disposition of the computational domains.

The grid is stretched in both streamwise and transverse directions, with clustering in the regions of high shear. Immediately downstream of the bluff body, the shear layer is resolved by about 20 grid points. For the LEMLES, 12 LEM cells are used in each LES cell. Using the predicted k^{sgs} and the local $\overline{\Delta}$, the maximum local sub-grid $Re_{\overline{\Delta}}$ is 130 and $\eta = 25$ x 10^{-6} m. Thus, scales down to about 3 η are resolved in the sub-grid. Due to heat release, the local $Re_{\overline{\Delta}}$ in most of the grid will be lower than this value and hence, the sub-grid resolution is considered acceptable.

The inflow velocity was 17.3 m/s with a 2 percent turbulence intensity under standard atmospheric conditions. The reference Reynolds number based on inflow velocity and bluff body height is $45,500$. The inflow consists of air in the cold flow case, and propane and air premixed mixture at an equivalence ratio of 0.65 for the reactive case. The simulations are carried out for 3 flow-through times before the flow statistics are collected, and the time averaged data presented herein are collected over a period equal to 5 flow-through times. Typically, cold flow simulations require about 75 single-processor hours for a single flow-through time,

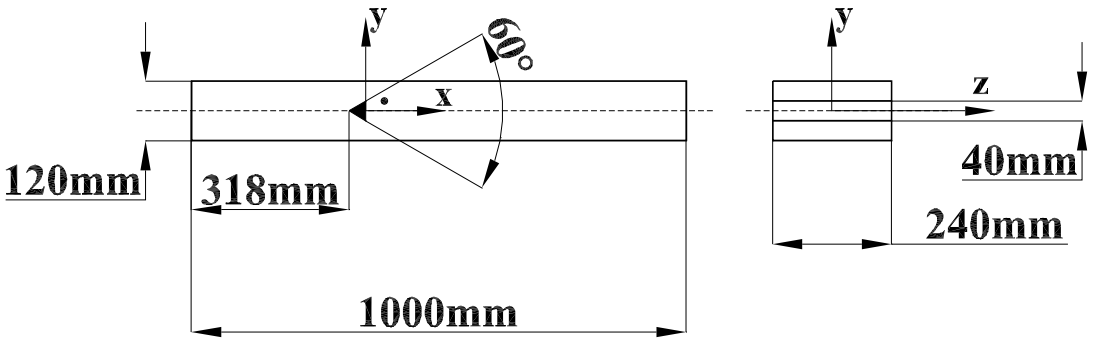

Figure 2. Schematic of the geometry. The solid symbol marks the position of the velocity probe used to capture the time signals in figures 3 and 8.

while the EBULES and LEMLES simulations take around 108 and 600 single-processor hours, respectively, on a Linux PC cluster.

V. Results and Discussion

A. Cold Flow

Figure 3 presents the Fast Fourier Transform of the kinetic energy contained in the axial velocity component, $E_{1,1}$. The energy spectrum presents a peak at 102.44 Hz, which represents the alternate vortex shedding frequency and compares well with the experimental value of $105Hz$ reported by Sjunesson et al.[4] After this maximum, the energy decay scales with the inertial range scaling,[40] $k^{-5/3}$. Here, k represents the wavenumber. The recovery of the $-5/3$ slope shows that the current grid is reasonable for LES.

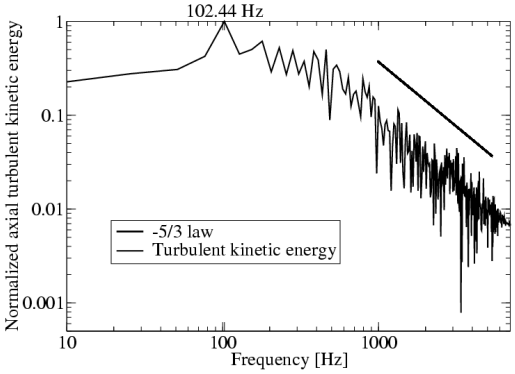

Figure 3. FFT of the axial turbulent kinetic energy for the cold flow, normalized by its maximum value.

The Strouhal number, defined as:

$$St = \frac{fa}{U_0} \tag{24}$$

is found to be equal to 0.24, in good agreement with earlier numerical[10] and experimental[4] studies. In the above, f is the shedding frequency, a is size of the bluff body, equal to 0.04 m, and U_0 is the inflow velocity, 17.3 m/s.

Figure 4 presents the instantaneous spanwise vorticity field in the recirculation region. The asymmetric vortex shedding occurs, as expected, from the two shear layers formed at the trailing edge of the prism in a von Karman vortex street pattern. The observed vortices develop as a result of the roll-up of the two vortex sheets formed at the trailing edges of the bluff body. Further downstream, the vortices break down into smaller eddies that eventually dissipate, due to vortex stretching and viscosity effects.

Comparison with the existing experimental data provides a better appraisal of the accuracy of the simulation. Figure 5 presents the normalized time-averaged axial velocity profile along the combustor centerline, behind the bluff body. The numerical result matches closely the experimental data. Immediately downstream of the bluff body, the velocity is negative and reaches a negative maximum of about 64% of the inflow velocity at around 0.75 a. The length of the recirculation region is about 1.25 a. After the end of the reverse flow area, the mean axial velocity increases upstream to gradually approach the free stream value, as the velocity deficit induced by the bluff body disappears.

Figure 6 shows several transverse profiles of the normalized time-averaged axial and transverse velocities at several locations downstream of the bluff body (the axial distance in figure 6 and thereafter is measured from the origin of the coordinate system shown in figure 2). The transverse velocity profiles reflect the vortical pattern discussed in figure 4. In terms of axial variation, as the vortices are shed at the backwall of

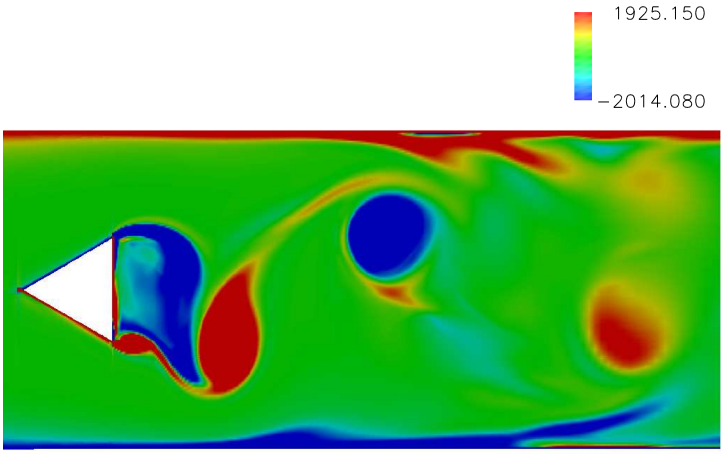

Figure 4. Instantaneous spanwise vorticity field for the cold flow.

the bluff body, their intensity increases over a distance of about 1.5 a, leading to an increase in the transverse velocity up to about 50% of the axial inflow value. After this peak, the transverse velocity decreases as the perturbation induced by the bluff body tends to disappear. The overall agreement with the experimental data[2] is good.

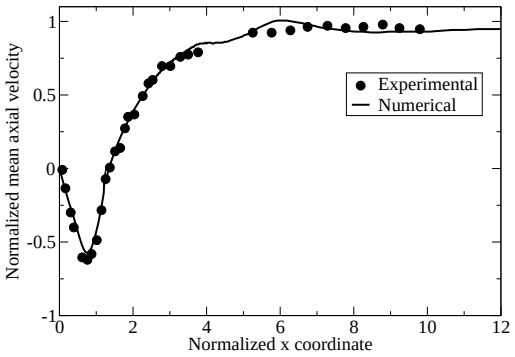

Figure 5. Centerline variation of the normalized time-averaged axial velocity for the cold flow. The velocity is normalized by the inflow value, and the distance is normalized by the bluff body size, a.

The variation along the transverse axis of the normalized axial, the transverse velocity fluctuation rms intensity and the Reynolds stress, $\overline{u'v'}$, are presented in figure 7 at the same five axial locations. The agreement with the measured experimental data remains good for both velocity components. Both axial and transverse fluctuations peak in the shear layers, at about 1.5 a downstream of the bluff body base, with a maximum value of about 65% of the inflow velocity, for the axial rms, and about 95% for the transverse rms. The velocity fluctuations have the tendency to become isotropic further downstream, as the influence of the large scale turbulent structures created by the obstruction becomes less important. The Reynolds stress peaks in the two shear layers that delimit the recirculation region, reaching a maximum of about 20% of the squared inflow velocity at 1.5 a, and decreases downstream, as turbulence decays and turbulent structures become less coherent.

B. Reactive Flow

As mentioned earlier, EBULES and and LEMLES simulation were carried out, and the results of the two simulations are compared against each other, as well as against the experimental data.

A Fast Fourier Transform is applied to the time signal of the kinetic energy contained in the axial velocity component, E_{11} (figure 8). The data in figure 8 were obtained through the LEMLES simulation and the position of the probe is shown in figure 2. The dominant frequency is found to be 138.57 Hz, which correlates well with the shedding frequency reported by earlier experimental[41] and numerical[10] studies. The Strouhal number (Eq. (24)) based on this frequency is 0.32, in good agreement with the LES data reported by Giacomazzi et al.[10] As in the cold flow, an important region of the energy spectrum recovers the $k^{-5/3}$ scaling suggests adequacy of the LES resolution.

The instantaneous spanwise vorticity and reaction rate, together with the time-averaged temperature fields are shown in figure 9 for EBULES and LEMLES, respectively. The instantaneous vorticity field in the

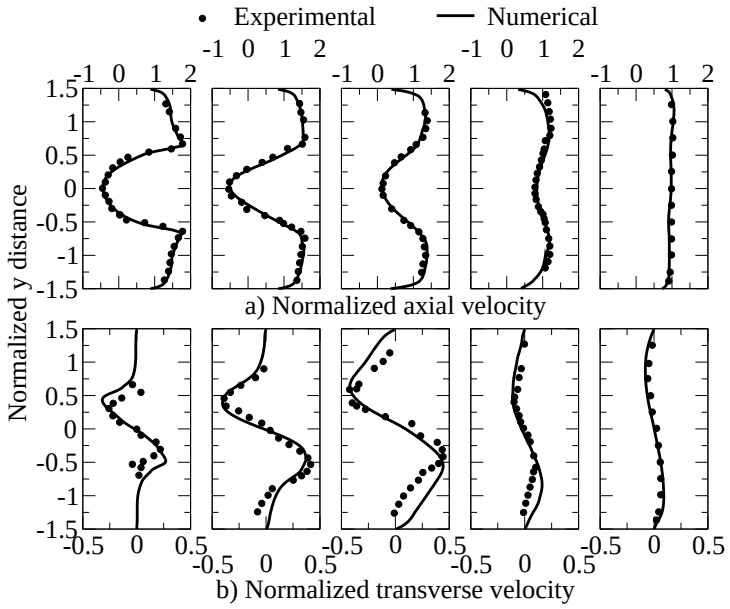

Figure 6. Transverse profiles of the time-averaged normalized axial and transverse velocities for the cold flow at the normalized axial locations, from left to right: 0.375 a, 0.95 a, 1.53 a, 3.75 a **and** 9.4 a**. The velocities are normalized by the inflow value,** U_0**, and the distance is normalized by the bluff body size,** a**.**

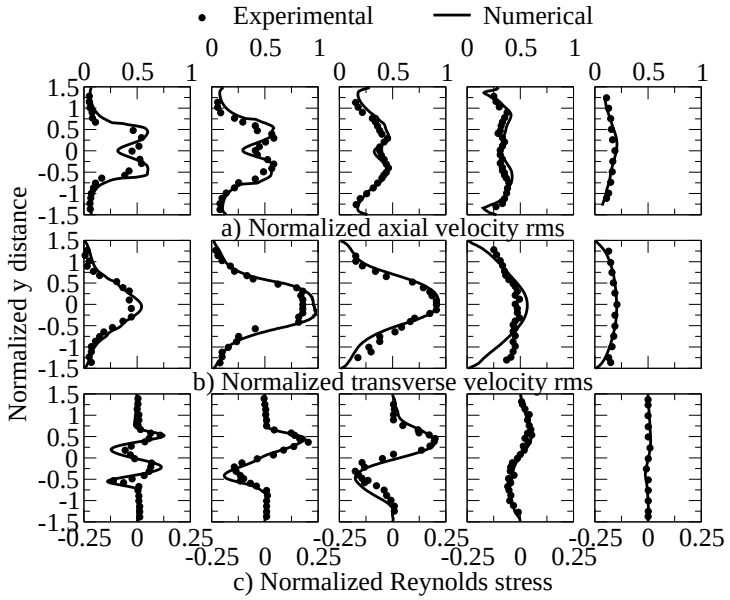

Figure 7. Transverse profiles of the normalized rms of the axial, of the transverse fluctuation intensity, and of the Reynolds stress for the cold flow, at the normalized axial locations, from left to right: 0.375 a, 0.95 a, 1.53 a, 3.75 a **and** 9.4 a**. The velocities are normalized by the inflow value,** U_0**, the Reynolds stress by** U_0^2**, and the distance is normalized by the bluff body size,** a**.**

reactive case is found to be quite different from the non-reactive result shown in figure 4 in several key points. McMurtry et al.[42] have shown that combustion occurs rapidly at the vortex core, causing the density to drop via thermal expansion. Since the angular momentum is conserved, an increased in the vortex area results in a decrease in its intensity. The strong baroclinic torque (shown in figure 10), resulting from non-aligned pressure and density gradients, strongly weakens the Kelvin-Helmholtz instability responsible for the von Karman street.[43]

The vortex shedding that occurs at the corners of the bluff body in the non-reactive case is now delayed,

and a pair of stationary vortices forms at the two edges.[44] Further downstream, flow instabilities in these stationary vortices lead to symmetric vortex shedding,[13] consistent with previous data.[44,45] In the initial phase of vortex development the vorticity is relatively low and the turbulent mixing and burning are reduced. Further downstream, the vortices undergo pairing and during this process the flame is wrinkled and its surface area increases rapidly, enhancing both turbulent mixing and combustion.

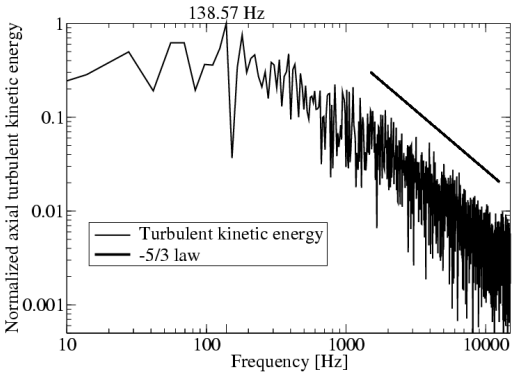

Figure 8. FFT of the axial turbulent kinetic energy for the reactive flow, normalized by its maximum value.

The vortical structures in the shear layers tend to wrap the flame surface around them,[46] as figure 9 indicates (here, the flame location is represented by the reaction rate contours). The flame predicted by LEMLES is significantly more wrinkled than the EBULES flame and the accompanying spreading of the wake is larger further downstream due to this effect in the LEMLES but is absent in the EBULES. The near field instantaneous temperature profile (not shown here) that follows the flame structure also follows the vorticity profile. Hence, the EBULES time-averaged temperature profile presents a reduced level of spreading when compared to LEMLES.

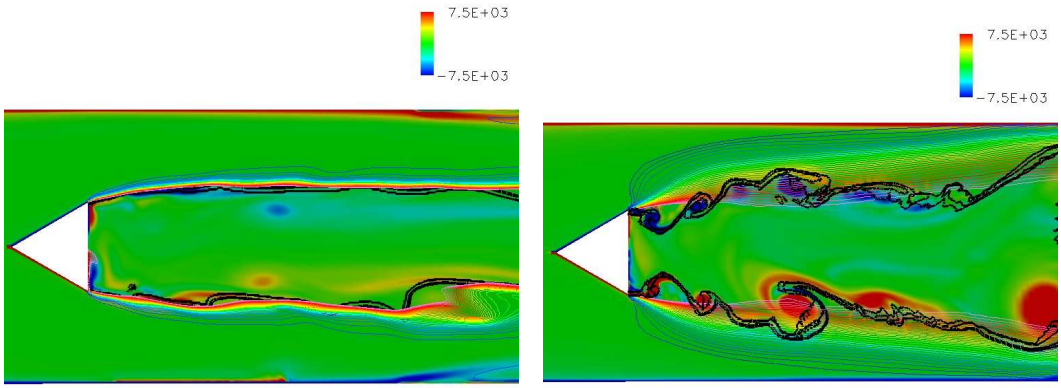

(a) EBULES (b) LEMLES

Figure 9. Instantaneous spanwise vorticity (solid color), instantaneous reaction rate (thick black line) and time-averaged temperature (color lines) for the reactive case.

Understanding the reasons behind the differences in the results of the two simulations and assessing which of the two discussed combustion models is a more accurate representation of the physical reality, requires some analysis of the simulated flame structure and of the underlying assumptions behind the two closures.

From a modelling standpoint, the fundamental assumption of the Eddy Break-Up model is that in the inertial subrange the time and length scales of the combustion process are separated from the times and scales characteristic for the turbulence. For the scale separation hypothesis to hold, the width of the inner layer of the flame reaction zone needs to be significantly smaller than the smallest eddy scale, the Kolmogorov scale. In order to understand the validity limits of the various proposed combustion models, the notion of *combustion regimes* has been introduced, as, for instance, by Peters.[17] For turbulent flames with turbulent intensities u' significantly larger than the laminar flame speed S_L, (in the present case u'/S_L in the flame region ranges between 25 and 70), two combustion regimes can be defined: the "Thin Reaction Zone" (TRZ) and the "Broken Reaction Zone" (BRZ) regimes. A value of the Karlovitz number, defined as $Ka = (l_F/\eta)^2$, where l_F is the flame thickness, and η the Kolmogorov length scale, of 100 is generally regarded[17] as the cutoff limit between the two.

From a physical standpoint, in TRZ, the smallest eddies can penetrate into the preheat zone of the flame and increase scalar mixing, but not into the inner layer (or reaction zone), thus maintaining the laminar

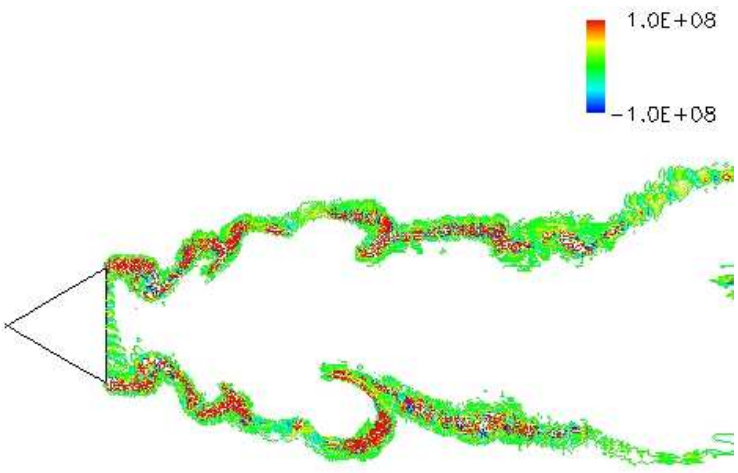

Figure 10. Instantaneous iso-contours of baroclinic torque spanwise component for the LEMLES reactive case.

structure of the reaction zone and maintaining the validity of the scale separation hypothesis. The influence of the small, unresolved eddies on the preheat zone is accounted for by the EBULES model, as it becomes mixing controlled in the regions of high turbulence.

However, for larger Karlovitz numbers, the combustion regime moves into the BRZ region, where the Kolmogorov size eddies are small enough to penetrate the inner layer of the flame and alter the laminar flame structure. In that case, the EBU assumptions are violated, and the model is expected to fail. The instantaneous Karlovitz number, computed as:[47]

$$Ka = \sqrt{\left(\frac{u'}{S_L}\right)^3 \frac{l_F}{\overline{\Delta}}} \tag{25}$$

exceeds the 100 limit over significant regions of the flame, especially in the two shear layers close downstream of the bluff body, as shown in figure 11. Therefore, in those regions, the EBU combustion model becomes unreliable. On the other hand, the LEM model simulates, at their appropriate length and time scales both the chemical reaction and turbulent stirring processes, thus capturing their detailed interaction. Therefore, LEMLES is able to handle the eddy penetration of the inner layer in the regions of high turbulent intensity. Figure 11 presents its instantaneous profile along the y axis at 0.015 m from the bluff body, as obtained from the LEMLES simulation.

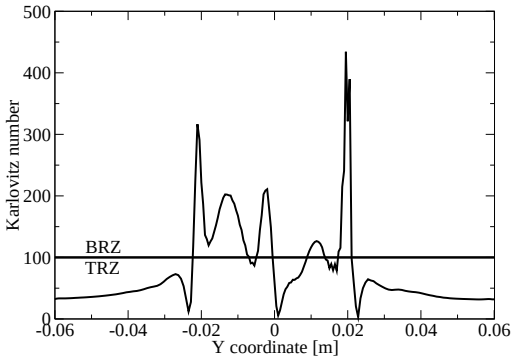

Figure 11. Transverse profiles of instantaneous Karlovitz number at axial location 0.015 **m.**

The penetration of the inner layer by small eddies causes the kinetics to become strongly affected by the turbulence. Furthermore, heat diffusion from the inner layer towards the preheat zone is significantly enhanced. Hence, the reaction zone thickness is overpredicted by EBULES and, as a thicker reaction zone is less susceptible to turbulent fluctuations,[48] EBULES predicts a much smoother flame than experimentally observed.[4] A comparative picture, showing a detail of the instantaneous EBULES and LEMLES reaction rates is presented in figure 12. It is obvious that even though the predicted flame thicknesses are relatively equal to each other in some regions, there are significant portions of the flame where LEMLES reaction zone is significantly thinner and those region also correspond to regions where the flame is strongly convoluted.

In terms of the mean velocities, the comparison with the existing experimental data shows good agreement for both simulations. Figure 13 presents the normalized axial velocity profile along the combustor

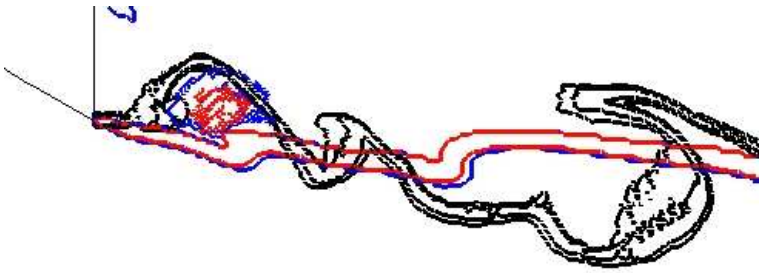

Figure 12. Instantaneous reaction rates. The color line represents the EBULES result and the black line the LEMLES.

centerline, behind the bluff body. Compared to the cold flow, the volumetric expansion caused by the chemical heat release causes an increase in the recirculation zone length and crossflow area, hence the residence time is increased, and the mass and the heat transfer across the shear layer are reduced due to a reduction in the turbulence intensity caused by the heat release and a decrease in density due to thermal expansion.[1] The length of the recirculation region is of about 3.75 a, and the maximum absolute value of the negative velocity reaches about 0.75 of the inflow velocity at about twice the size of the bluff body, indicating a more significant flow reversal effect than in the cold flow, in agreement with the experimental data. The far-field free stream velocity is about 3 times larger than the inflow velocity, due to the addition of chemical energy through combustion. Both combustion models yield equally accurate results, although LEMLES appears to show slightly better agreement, which is due to a better temperature prediction in the far field, as it shown later.

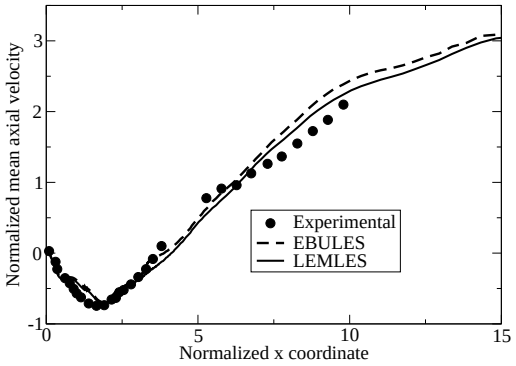

Figure 13. Centerline variation of the normalized time-averaged axial velocity for the reactive flow.

In the transverse direction, the accuracy is also acceptable, as seen in figure 14 that shows profiles of the time-averaged normalized axial and transverse velocity at several locations downstream of the bluff body. As mentioned before, the negative velocity region is found to be wider than for a non-reactive flow. In the near field, LEMLES predicts a more accurate axial velocity in the stream by-passing the bluff body, correlating well with the improved temperature predictions, to be shown later. Also, far downstream, the centerline velocity becomes over-predicted by EBULES, indicating that the predicted acceleration rate is slightly off.

In the case of the transverse component of the time-averaged velocity, the agreement with the experimental data[3] is generally good. The large scale vortical structures created by the presence of the bluff body decrease in intensity with the distance from the obstruction, as the wake momentum deficit diminishes and the flow tends to recover its initial axial direction. Generally, the magnitude of the transverse component is lower than in the non-reactive case, as an effect of the reduced vorticity magnitudes observed in figure 9. The maximum transverse velocity is about 30% of the inflow velocity, and is achieved closer to the bluff body, at about 0.4 a, due to the increased viscous effects resulting from the higher temperature. A notable feature of the flow field is the sudden decrease of the transverse velocity at the flame front, not captured in the non-reactive data. This behavior correlates with the pair of stationary, counter-rotating vortices mentioned earlier. The effect disappears further downstream, where the intensity and the coherence of the vortices weakens.

The axial, the transverse velocity fluctuations and the Reynolds stress $\overline{u'v'}$ along the transverse axis are presented in figure 15. For the axial component, the EBU model tends to underpredict the velocity fluctuations at the centerline, while LEMLES predicts values in significantly better agreement with the experimental data due to the more accurate modelling of the flame - turbulence interaction. In the shear layer, the velocity fluctuations are generally overpredicted by both models, although the overprediction

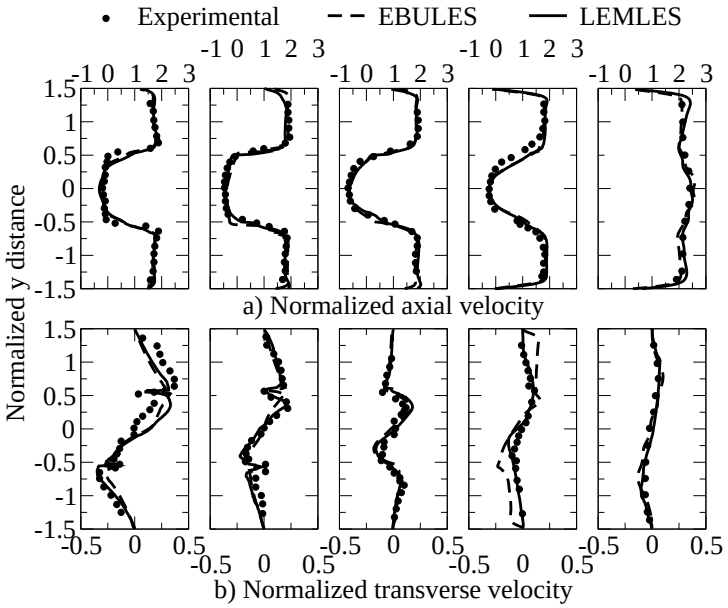

Figure 14. Transverse profiles of the normalized time-averaged axial and transverse velocities for the reactive flow, at the normalized axial locations, from left to right: 0.375 a, 0.95 a, 1.53 a, 3.75 a.

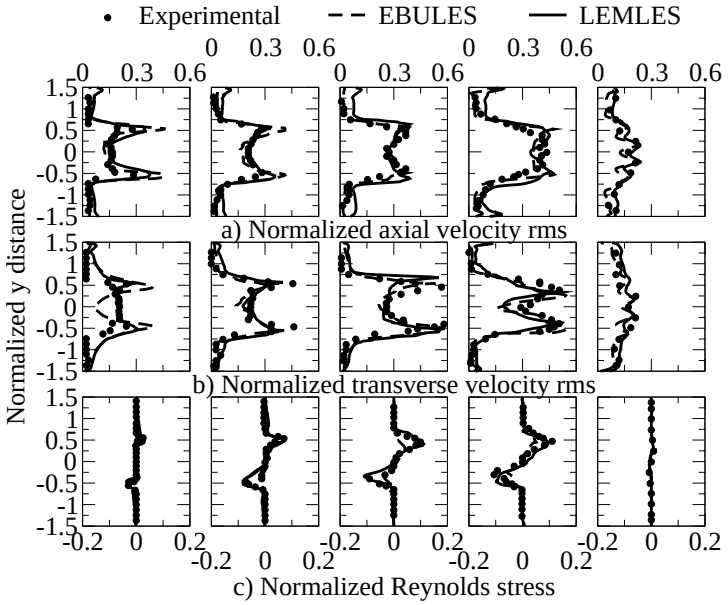

Figure 15. Transverse profiles of the normalized rms of the axial, of the transverse fluctuation intensity, and of the Reynolds stress for the reactive flow, at the normalized axial locations, from left to right: 0.375 a, 0.95 a, 1.53 a, 3.75 a **and** 9.4 a.

decreases downstream, especially for LEMLES. However, the overprediction of the EBULES is about twice as large in the near field when compared to LEMLES for both axial and transverse fluctuations.

The Reynolds stress peaks in the two shear layers created at the bluff body sharp corners, at a value of about 10% of the squared inflow velocity, in agreement with the experimental observations. Again, the LEMLES provides a more accurate result.

As first observed in figure 9, the LEMLES simulation results presents an increased spreading of the burnt region, when compared to EBULES. This is also evident in the transverse time-averaged normalized temperature profiles, shown in figure 16 at axial locations 3.75 a, 8.75 a and 13.75 a. In figure 16, the

temperature is normalized by the inflow value, and the distance is normalized by the bluff body size, a. As a consequence of the overestimated flame thickness discussed earlier, the EBULES flame is slower to respond to the turbulent fluctuations, and the intermittency effect is not captured accurately. As a consequence, the turbulent flame brush is not captured accurately by EBULES and the spreading rate of the time-averaged temperature profile is underestimated.

Also, EBULES tends to underpredict the centerline values by as much as 10%. It can be noted that the centerline region is also the region of low turbulent kinetic energy and EBULES will predict here a reduced turbulent mixing rate. However, the experimental data show that the temperature maintains its high value over a large portion of the domain, so even with a reduced mixing rate the premixed reactants entrained in this region should burn at a high rate. The LEM model, on the other hand, avoids estimating the controlling rate and simulates the involved processes, thus allowing for a more accurate prediction of the temperature. The more accurate prediction of heat release results in more accurate spreading rates, which is reflected in the velocity field, as discussed earlier. These results demonstrate the subtle and global effects of using a more comprehensive combustion and mixing model as in LEMLES.

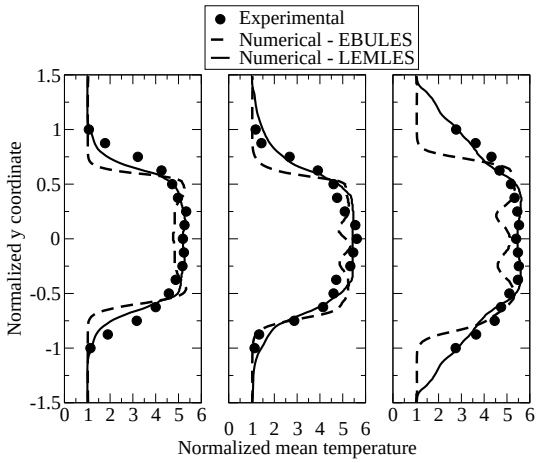

Figure 16. Transverse profiles of the normalized time-averaged temperature for the reactive flow, at the normalized axial locations, from left to right: 3.75 a, 8.75 a **and** 13.75 a.

VI. Conclusions

In this study, LES of both non-reactive and reactive flows are conducted for a bluff body stabilized flow. Anti-symmetric vortex shedding, at a frequency of 102.44 Hz is observed, and the time-averaged and the rms fluctuations of axial and transverse velocities are found in good agreement with the experiments for the non-reactive data.

In the reactive studies, two models are used and compared. The spanwise vorticity field is found to be qualitatively different from the non-reactive case. The thermal expansion in the vortex core and the baroclinic torque effect weaken the Kelvin-Helmoltz instability and suppress the formation of the von Karman vortex street. Symmetric vortex shedding induced by fluctuations in the density and velocity fields occurs further downstream, at a frequency of 138.57 Hz, which agrees with earlier data. The vorticity and the temperature fields are significantly more accurately predicted in the LEMLES approach and this results in an improved prediction of the scalar field.

Besides the EBULES results, previous numerical simulations of similar geometries[4,10,13,44] have all failed to capture the correct experimentally measured spreading rate. A common feature of these studies was the laminar chemistry assumption embedded in the combustion models (Eddy Dissipation Model,[4,10] or EBU[13,44]). The present study indicates that the laminar chemistry is affected by small eddies penetrating the flame front and the scale separation hypothesis is invalid over an important region of the flame. Consequently, the flame thickness predicted by the EBULES is over-predicted rendering the flame front less susceptible to turbulent fluctuations in the flow. Hence, flame surface wrinkling is significantly more pronounced in LEMLES, the flame structure more complex, and the far field spreading of the wake is closer to the experimental observations. The time-averaged temperature in the low turbulence centerline region is

underestimated by EBULES, due to underpredicted turbulent mixing rates in the region. As a consequence, the velocity fluctuations are also better predicted by the LEMLES, when compared to EBULES.

Acknowledgments

This work was partially supported by the Pratt & Whitney Company.

References

[1]Ozawa, R. I., "Survey of Basic Data on Flame Stabilization and Propagation for High Speed Combustion Systems," Tech. Rep. Technical Report AFAPL-TR-70-81, The Maquardt Company, 1971.

[2]Sjunesson, A., Nelson, C., and Max, E., "LDA Measurements of Velocities and Turbulence in a Bluff Body Stabilized Flame," *Technical Report S-461 81*, 1991.

[3]Sjunesson, A., Olovsson, S., and B., S., "Validation Rig - A Tool for Flame Studies," *Technical Report 9370-3088*, 1991.

[4]Sjunesson, A., Henriksson, R., and Lofstrom, C., "CARS Measurements and Visualization of Reacting Flows in Bluff Body Stabilized Flame," *AIAA - 92 - 3650*, 1992.

[5]Bai, X. and Fuchs, L., "Modeling of Turbulent Reactive Flows Past a Bluff Body: Assessment of Accuracy and Efficiency," *Computers and Fluids*, Vol. 23, No. 3, 1994, pp. 507–521.

[6]Stone, C. and Menon, S., "LES of Partially-Premixed Unsteady Combustion," *AIAA-2003-0316*, 2003.

[7]Menon, S., "Acoustic-Vortex-Flame Interactions in Gas Turbine Combustors," *Combustion Instabilities in Gas Turbine Engines: Operational Experience, Fundamental Mechanisms, and Modeling*, edited by T. Lieuwen and V. Yang, Vol. 210, AIAA Progress in Aeronautics and Astronautics, 2005, pp. 277–314.

[8]Fureby, C., "On Sub Grid Scale Modeling in Large Eddy Simulations of Compressible Fluid Flow," *Physics of Fluids*, Vol. 8, No. 5, 1996, pp. 1301–1311.

[9]Fureby, C., "A Computational Study of Combustion Instabilities Due to Vortex Shedding," *Proceedings of the Combustion Institute*, Vol. 28, 2000, pp. 783–791.

[10]Giacomazzi, E., Battaglia, V., and Bruno, C., "The Coupling of Turbulence and Chemistry in a Premixed Bluff-Body Flame as Studied by LES," *Combustion and Flame*, Vol. 138, 2004, pp. 320–335.

[11]Menon, S., Stone, C., and Patel, N., "Multi-Scale Modeling for LES of Engineering Designs of Large - Scale Combustors," *AIAA-2004-0157*, 2004.

[12]Kim, W. W. and Menon, S., "A New Incompressible Solver for Large - Eddy Simulations," *International Journal of Numerical Methods in Fluids*, Vol. 31, 1999, pp. 983–1017.

[13]Fureby, C. and Moller, S. I., "Large Eddy Simulations of Chemically Reactive Flows Applied to Bluff Body Stabilized Flames," *AIAA Journal*, Vol. 33, No. 12, 1995, pp. 2339–2347.

[14]Poinsot, T. J. and Veynante, D., *Theoretical and Numerical Combustion*, Edwards, 2001.

[15]Pope, S. B., "Computations of Turbulent Combustion: Progress and Challenges," *Twenty - Third Symposium (International) on Combustion*, 1990, pp. 591–612.

[16]Sethian, F. A., *Level Set Methods. Evolving Interfaces in Geometry, Fluid Mechanics, Computer Vision and Material Science*, Cambridge University Press. Cambridge. U.K., 1996.

[17]Peters, N., *Turbulent Combustion*, Cambridge University Press, Cambridge, U.K., 2000.

[18]Magnussen, B. F. and Hjertager, B. H., "On Mathematical Models of Turbulent COmbustion with With Special Emphasis on Soot Formation and Combustion," *Sixteenth Symposium (International) on Combustion*, 1977, pp. 719–729.

[19]Westbrook, C. K. and Dryer, F. L., "Simplified Reaction Mechanisms for the Oxidation of Hydrocarbon Fuels in Flames," *Combustion Science and Technology*, Vol. 27, 1981, pp. 31–43.

[20]Kerstein, A. R., "Linear-Eddy Modeling of Turbulent Transport II," *Combustion and Flame*, Vol. 75, 1989, pp. 397–413.

[21]Menon, S., McMurtry, P. A., and Kerstein, A. R., "A Linear Eddy Mixing Model for Large Eddy Simulation of Turbulent Combustion," *LES of Complex Engineering and Geophysical Flows. Ed. B. Galperin and S. Orszag*, 1993.

[22]Menon, S. and Calhoon, W. H., "Subgrid Mixing and Molecular Transport Modeling for Large Eddy Simulations of Turbulent Reacting Flows," *Proceedings of the Combustion Institute*, Vol. 26, 1996, pp. 59–66.

[23]Chakravarthy, V. K. and Menon, S., "Linear - Eddy Simulations of Reynolds and Schmidt Number Dependencies in Turbulent Scalar Mixing," *Physics of Fluids*, Vol. 13, 2001, pp. 488–499.

[24]Sankaran, V. and Menon, S., "LES of Scalar Mixing in Supersonic Shear Layers," *Proceedings of the Combustion Institute*, Vol. 30, No. 2, 2005, pp. 2835–2842.

[25]Chakravarthy, V. K. and Menon, S., "Subgrid Modeling of Premixed Flames in the Flamelet Regime," *Flow, Turbulence and Combustion*, Vol. 65, 2000, pp. 23–45.

[26]Sankaran, V. and Menon, S., "Subgrid Combustion Modeling of 3-D Premixed Flames in the Thin-Reaction-Zone Regime," *Proceedings of the Combustion Institute*, Vol. 30, No. 1, 2005, pp. 575–582.

[27]Eggenspieler, G. and Menon, S., "Combustion and Emission Modelling near Lean Blow-Out in a Gas Turbine Engine," *Progress in Computational Fluid Dynamics*, Vol. 5, No. 6, 2005, pp. 281–297.

[28]Calhoon, W. H., Menon, S., and Goldin, G., "Comparison of Reduced and Full Chemical Mechanisms for Nonpremixed Turbulent H2 - Air Jet Flames," *Combustion Science and Technology*, Vol. 104, 1995, pp. 115–141.

[29]Menon, S., "CO Emission and Combustion Dynamics Near Lean Blow-Out in Gas Turbine Engines," *ASME-GT2004-53290*, 2004.

[30]Menon, S. and Patel, N., "Subgrid Modeling for LES of Spray Combustion in Large-Scale Combustors," *AIAA Journal*, 2005, pp. In Press.

[31]Sankaran, V., Porumbel, I., and Menon, S., "Large-Eddy Simulation of a Single-Cup Gas Turbine Combustor," *AIAA-2003-5083*, 2003.

[32]Smith, T. M. and Menon, S., "One-dimensional simulations of freely propagating turbulent premixed flames," *Combustion Science and Technology*, Vol. 128, 1996, pp. 99–130.

[33]Yakhot, V., "Propagation Velocity of Premixed Turbulent Flames," *Combustion Science and Technology*, Vol. 60, 1988, pp. 191–214.

[34]Pocheau, A., "Scale Invariance in Turbulent Flame Propagation," *Physical Review E*, Vol. 49, 1994, pp. 1109–1122.

[35]Menon, S., "Modeling Combustion Dynamics and Pollutatnt Formation near Lean Blow Out in Gas Turbine Combustor," *AIAA-2003-4496*, 2003.

[36]Menon, S. and Kerstein, A. R., "Stochastic Simulation of the Structure and Propagation Rate of Turbulent Premixed Flames," *Proceedings of the Combustion Institute*, Vol. 24, 1992, pp. 443–450.

[37]Jameson, A., Schmidt, W., and Turkel, E., "Numerical Solutions of the Euler Equations by Finite Volume Methods with Runge Kutta Time Stepping Schemes," *AIAA-81-1259*, 1981.

[38]Jameson, A., "Time Dependent Calculations Using Multigrid, with Applications to Unsteady Flows Past Airfoils and Wings," *AIAA-91-1596*, 1991.

[39]Baum, M., Poinsot, T. J., Haworth, D. C., and Darabiha, N., "Direct Numerical Simulation of $H_2/O_2/N_2$ Flames With Complex Chemistry in Two-Dimensional Turbulent Flows," *Journal of Fluid Mechanics*, Vol. 281, 1994, pp. 1–32.

[40]Pope, S. B., *Turbulent Flows*, Cambridge University Press, 2000.

[41]Fureby, C., "Large Eddy Simulation of Combustion Instabilities in a Jet Engine Afterburner Model," *Combustion Science and Technology*, Vol. 161, 2000, pp. 213–244.

[42]McMurtry, P. A., Jou, W. H., Riley, J. J., and Metcalfe, R. W., "Direct Numerical Simulations of a Reacting Mixing Layer with Chemical Heat Release," *AIAA Journal*, Vol. 26, No. 6, 1985, pp. 962–970.

[43]Chakravarthy, V. K. and Menon, S., "Large-Eddy Simulations of Confined Bluff-Body Stabilized Highly Turbulent Premixed Flames," *3rd ASME/JSME Joint Fluids Engineering Conference. San Francisco, CA, July 18-23*, , No. FEDSM99-7798, 1999.

[44]Fureby, C. and Lofstrom, C., "Large-eddy Simulations of Bluff - Body Stabilized Flames," *Twenty - Fifth Symposium (International) on Combustion*, 1994, pp. 1257–1264.

[45]Veynante, D., Piana, J., Duclos, J. M., and Martel, C., "Experimental Analysis of Flame Surface Density Models for Premixed Turbulent Combustion," *Twenty - Sixth Symposium (International) on Combustion*, 1996, pp. 1249–1256.

[46]Poinsot, T. J., Veynante, D., and Candel, S., "Quenching Processes and Premized Turbulent Combustion Diagrams," *Journal of Fluid Mechanics*, Vol. 228, 1991, pp. 561–606.

[47]Pitsch, H. and Duchamp De Lageneste, L., "Large - Eddy Simulation of Premized Turbulent Combustion using a Level - Set Approach," *Twenty - Ninth Symposium (International) on Combustion*, 2002, pp. 2001–2008.

[48]Chakravarthy, V. K. and Menon, S., "Large - Eddy Simulations of Turbulent Premixed Flames in the Flamelet Regime," *Combustion Science and Technology*, Vol. 162, 2000, pp. 1–48.